RSC Advances

PAPER



Cite this: *RSC Adv.*, 2023, **13**, 19288

# Effective adsorption of Pb(II) from wastewater using $MnO_2$ loaded MgFe-LD(H)O composites: adsorption behavior and mechanism†

Yongxiang Huang,‡[ab] Xiangping Luo,‡[ab] Chongmin Liu, *[ab] Shaohong You,*[ab] Saeed Rad[ab] and Litang Qin[ab]

Pb(II) adsorption by $MnO_2$/MgFe-layered double hydroxide ($MnO_2$/MgFe-LDH) and $MnO_2$/MgFe-layered metal oxide ($MnO_2$/MgFe-LDO) materials was experimentally studied in lab-scale batches for remediation property and mechanism analysis. Based on our results, the optimum adsorption capacity for Pb(II) was achieved at the calcination temperature of 400 °C for $MnO_2$/MgFe-LDH. Langmuir and Freundlich adsorption isotherm models, pseudo-first-order and pseudo-second-order kinetics, Elovich model, and thermodynamic studies were used for exploring the Pb(II) adsorption mechanism of the two composites. In contrast to $MnO_2$/MgFe-LDH, $MnO_2$/MgFe-$LDO_{400\ °C}$ has a stronger adsorption capacity and the Freundlich adsorption isotherm model ($R^2$ > 0.948), the pseudo-second-order kinetic model ($R^2$ > 0.998), and the Elovich model ($R^2$ > 0.950) provide great fits to the experimental data, indicating that the adsorption occurs predominantly *via* chemisorption. The thermodynamic model suggests that $MnO_2$/MgFe-$LDO_{400\ °C}$ is spontaneously heat-absorbing during the adsorption process. The maximum adsorption capacity of $MnO_2$/MgFe-$LDO_{400\ °C}$ for Pb(II) was 531.86 mg $g^{-1}$ at a dosage of 1.0 g $L^{-1}$, pH of 5.0, and temperature of 25 °C. Through characterization analysis, the main mechanisms involved in the adsorption process were precipitation action, complexation with functional groups, electrostatic attraction, cation exchange and isomorphic replacement, and memory effect. Besides, $MnO_2$/MgFe-$LDO_{400\ °C}$ has excellent regeneration ability in five adsorption/desorption experiments. The above results highlight the powerful adsorption capacity of $MnO_2$/MgFe-$LDO_{400\ °C}$ and may inspire the development of new types of nanostructured adsorbents for wastewater remediation.

Received 7th May 2023
Accepted 19th June 2023

DOI: 10.1039/d3ra03035k

rsc.li/rsc-advances

## 1. Introduction

Improper discharge of industrial waste results in a large number of pollutants entering into the environment, contaminating the soil, atmosphere, and water bodies. Lead, as one of the most toxic pollutants in water, comes from industrial wastewater discharge, atmospheric particulate matter deposition, water leaching seepage of industrial waste slag and tailings, *etc.*[1] Discharged lead exists in the environment in various forms including $Pb^{2+}$, $Pb(OH)^{+}$, $Pb(OH)_2$, $Pb(OH)^{3-}$, $Pb(OH)_4^{2-}$, *etc.*[2] However, any form of lead presents high toxicity to the human body because as a persistent, long-lasting, and non-biodegradable contaminant, it can cause widespread brain damage.[3] Therefore, high concentrations of lead in the environment pose a significant threat to humans and the environment. Typical methods for treating lead-containing wastewater include chemical precipitation,[4] membrane separation technology,[5] ion exchange,[6] adsorption,[7] biochemical methods,[8] *etc.* Adsorption is a prominent approach among them because of its simplicity, high removal efficiency, and regenerative nature. Commonly used adsorbents include activated carbon,[9] activated alumina,[10] ferric hydroxide and, oxides,[11] zero-valent iron,[12] zeolites,[13] *etc.*

Nanoparticles are gaining popularity in environmental remediation because they may provide numerous and easily accessible metal sites, allowing them to be employed on a broad scale.[14] Among them, mineral-based materials are potential sorbents with exceptional characteristics that have been applied for the removal of various heavy metal ions through physisorption, ion exchange, surface complexation, and precipitation.[15] Layer double hydroxides (LDHs), as anionic or hydrotalcite-like clays, have attracted remarkable attention in ion exchange, catalysis, adsorption, and other fields.[16] Although scarce in nature, but it can be manufactured in the laboratory in large amounts using precursors.[17] Besides, LDHs nanomaterial are biocompatible and non-toxic, making them the perfect

[a]*College of Environmental Science and Engineering, Guilin University of Technology, Guilin 541004, China. E-mail: chongmin@glut.edu.cn; youshaohong@glut.edu.cn*
[b]*Guangxi Key Laboratory of Theory & Technology for Environmental Pollution Control, Guilin University of Technology, Guilin 541004, China*

† Electronic supplementary information (ESI) available. See DOI: https://doi.org/10.1039/d3ra03035k

‡ These authors contributed equally to this work.

green material. These are also resistant to heat, radiation, acids, bases, and their variable interlayer can accommodate molecules of different sizes, which make them promising materials for a wide range of applications in ecology, biology, and applied chemistry.[18] What's more, their calcined products, layered double oxides (LDO) are also employed as adsorbents to remove metal pollutants from water because of their memory effect, surface defects, homogenous metal cation dispersion, abundant active centers, thermal, and chemical stability.[19] For example, Xiangli Xie, *et al.* synthesized MgAl-LDO by calcination of MgAl-LDH, the process involved a fast adsorption within three hours and the adsorption capability for lead is 6.26 mg $g^{-1}$.[20] Yuanyuan Yang, *et al.* find AF-LDH and AF-LDO could efficiently remove trace pollutants (10–100 μg $L^{-1}$) from multi-component solution, especially for AF-LDO, which could completely remove Pb(II), Cu(II), Zn(II), Cd(II), As(V) six trace metal(loid)s.[21]

However, stacking is easy to occur during the synthesis of LDHs, which can reduce the adsorption capability of LDHs. Therefore, there have been a large number of studies related to LDHs material loading other materials to improve the adsorption of heavy metals, such as metal–organic frameworks (MOFs),[22] chitosan,[23] magnetic graphene oxide (GO),[24] *etc.* Manganese dioxide ($MnO_2$) with large surface area, and high adsorption ability, and has been extensively used for the removal of heavy metals.[25] Meng Xu, *et al.*[26] used hydrated manganese dioxide (HMO), synthesized by redox of potassium permanganate and hydrogen peroxide, as an adsorbent for the removal of Pb(II). The uptake of Pb(II) by HMO was correlated with increasing surface hydroxyl group content. Good results have been achieved in adsorbing trace heavy metal ions $Cu^{2+}$, $Pb^{2+}$, $Cr^{3+}$, $Hg^{2+}$, As(V), and $Cd^{2+}$ in water.[27–29] However, $MnO_2$ is difficult to crystallize during synthesis and undergoes reduction easily. The adsorption properties of $MnO_2$ were greatly improved by calcination, doping, and modification. Some precursor studies have proven that loading on a suitable carrier, to form the compound materials could be an efficient way to overcome the disadvantages of $MnO_2$ and improve its application.[28,29] In our previous work,[30] the $MnO_2$/MgFe-LDH and $MnO_2$/MgFe-$LDO_{400\ ^\circ C}$ were facilely synthesized and tested for the removal of As(III) and proved that the combined materials have an excellent removal capacity (53.79 mg $g^{-1}$), functional groups of Mn–O or Fe–O on the surface of $MnO_2$/MgFe-LDH and $MnO_2$/MgFe-$LDO_{400\ ^\circ C}$ can form complexes with As(III). Importantly, it shows that our composite materials can be applied to water pollution of different heavy metals. Danni Chen *et al.*[31] combine the oxidation performance of manganese oxide and the high adsorption capacity of iron oxide to remove lead ions. Hui Li *et al.*'s findings explain that iron oxides on the surface of $Fe^0$, such as goethite (FeOOH), provide binding sites for Pb(II).[32] We assumed that the mechanism of adsorption of As(III) may also play a role for Pb(II), therefore we tried to use this material to adsorb Pb(II). Until now, the MgFe-LDH had fascinated a great amount of attention as a metal adsorption material.[30,33] Complexation of Pb(II) with oxygen-containing groups and interlayer $OH^-$ ions mainly contributed to extract Pb(II) from wastewater.[34] Synthesis of MgFe-LDO from MgFe-LDH could be facile designed for improving the adsorption sites with memory effect, which may attract many interests in extracting pollutants for environmental decontamination. Thus, it is hypothesized that the $MnO_2$/MgFe-LDO could be obtained from $MnO_2$/MgFe-LDH, which may perform a memory effect on Pb(II) adsorption. Also, the Mn–O chemical bond may play an important role in the complexation of functional groups adsorbed by Pb(II).

In the present study, a precursor of MgFe-LDH was synthesized by the co-precipitation method, and then potassium permanganate and manganese chloride solution were added to load the surface of material with $MnO_2$, denoted as $MnO_2$/MgFe-LDH. Subsequently, the composite of $MnO_2$/MgFe-LDH was calcined at 400 °C for 5 h to form $MnO_2$/MgFe-$LDO_{400\ ^\circ C}$. The adsorptive performances of the calcined and uncalcined materials were explored for the uptake of Pb(II). The effect of various sorption factors, such as solution pH, temperature, kinetics, and isotherm, *etc.* were investigated in detail. The reusability study of $MnO_2$/MgFe-LDH and $MnO_2$/MgFe-$LDO_{400\ ^\circ C}$ was also studied. Finally, an in-depth investigation on Pb(II) adsorption are analyzed.

## 2. Materials and methods

### 2.1 Chemicals

The chemicals $Mg(NO_3)_2 \cdot 6H_2O$, $Fe(NO_3)_3 \cdot 9H_2O$, $KMnO_4$, $MnCl_2 \cdot 4H_2O$, $Pb(NO_3)_2$, NaOH, $Na_2CO_3$, NaCl, HCl, $H_2SO_4$, and $HNO_3$ were purchased from Xilong Scientific Co., Ltd. The chemical reagents used in this study were of analytical grade, and solutions were prepared using deionized (DI) water.

### 2.2 Material synthesis methods

The synthesis and characterization of the materials of $MnO_2$/MgFe-LDH and $MnO_2$/MgFe-$LDO_{400\ ^\circ C}$ used in this study has been described in our previous work.[30]

### 2.3 Material selection

Briefly, 30 mg of the $MnO_2$, MgFe-LDH, $MnO_2$/MgFe-LDH, $MnO_2$/MgFe-$LDO_{400\ ^\circ C}$, $MnO_2$/MgFe-$LDO_{500\ ^\circ C}$, and $MnO_2$/MgFe-$LDO_{600\ ^\circ C}$ were added to 30 mL of 500 mg L per Pb(II) solution. After the reaction, residual Pb(II) concentration was measured using inductively coupled plasma emission spectrometry (ICP-OES).

### 2.4 Bath adsorption experiments

The influence of the dosage (500 and 1000 mg $L^{-1}$, 0.5–3.0 g $L^{-1}$), initial solution pH value (500 mg $L^{-1}$, 2.0–8.0), contact time (500, 800 and 1000 mg $L^{-1}$, 5–3960 min), and initial concentration of Pb(II) (100–1500 mg $L^{-1}$) at three temperature (25 °C, 35 °C, and 45 °C) on the removal efficiency of Pb(II) ions by $MnO_2$/MgFe-LDH and $MnO_2$/MgFe-$LDO_{400\ ^\circ C}$ were tested. The adsorption experiments were carried out in a constant temperature shaker at a speed of 160 rpm. The solution was removed and passed through a 0.45 μm aqueous filter membrane after the adsorption equilibrium, and then the residual Pb(II) concentration was measured by ICP-OES.

All adsorption experiments were conducted with three replicates, the adsorbed amount of the Pb(II) on materials, $Q_e$ (mg $g^{-1}$) and removal efficiency of Pb(II) were assessed using eqn (1) and (2), respectively.

$$Q_e = \frac{C_0 - C_e}{m} \times V \quad (1)$$

$$\text{Removal rate } (\%) = \frac{C_0 - C_e}{C_0} \times 100 \quad (2)$$

where $m$ (mg) is the mass of the adsorbent and $V$ (mL) is the volume of the solution, $C_0$ and $C_e$ are the initial and equilibrium concentrations of Pb(II) (mg $L^{-1}$), respectively.

The kinetic adsorptions were fitted with pseudo-first-order kinetic model, pseudo-second-order kinetic model and Elovich models by the equations of (3)–(5):[35,36]

$$\lg(Q_e - Q_t) = \lg Q_e - \frac{K_1}{2.303} t \quad (3)$$

$$\frac{t}{Q_t} = \frac{1}{K_2 {Q_e}^2} + \frac{t}{Q_e} \quad (4)$$

$$Q_t = \frac{1}{\beta} \ln(\alpha\beta) + \frac{\ln t}{\beta} \quad (5)$$

where $K_1$ is the primary adsorption rate constant; $K_2$ is the secondary adsorption rate constant; $Q_e$ is the adsorption capacity at adsorption equilibrium (mg $g^{-1}$); $Q_t$ is the adsorption capacity at time $t$ (mg $g^{-1}$); $t$ is the adsorption time; $\beta$ (g $mg^{-1}$) is the desorption coefficient, and $\alpha$ (mg $g^{-1}$ $min^{-1}$) is the initial adsorption coefficient.

The isotherm adsorptions were fitted with Langmuir and Freundlich models by the equations of (6) and (7):[37,38]

$$Q_e = \frac{Q_m K_L c_e}{1 + K_L c_e} \quad (6)$$

$$Q_e = K_F c_e^{\frac{1}{n}} \quad (7)$$

where $Q_e$ (mg $g^{-1}$) is the adsorption capacity of the target pollutants in the adsorption equilibrium, $Q_m$ (mg $g^{-1}$) is the adsorption capacity of the mixture for target pollutants, $C_e$ (mg $L^{-1}$) is the equilibrium concentration of Pb(II) on the clay composites, $n$ is a characteristic constant related to the adsorption strength or favorable adsorption degree, and lastly, $K_L$ (L $mg^{-1}$) and $K_F$ (mg $g^{-1}$) are the Langmuir and Freundlich constants, respectively.

The thermodynamic adsorption was used to calculated enthalpy change ($\Delta H$, kJ $mol^{-1}$), Gibbs free energy ($\Delta G$, kJ $mol^{-1}$) and entropy change ($\Delta S$, J $mol^{-1}$ $K^{-1}$) by using the following equations:[54]

$$K_e = \frac{q_e}{c_e} \quad (8)$$

$$\Delta G = \Delta H - T\Delta S \quad (9)$$

$$\Delta G = -RT \ln K_e \quad (10)$$

$$\ln K_e = \frac{\Delta S}{R} - \frac{\Delta H}{RT} \quad (11)$$

where $K_e$ (L $g^{-1}$) is the equilibrium constant of materials adsorption; and $R$ (8.31 J $mol^{-1}$ $K^{-1}$) is gas constant.

### 2.5 Regeneration experiment

In order to select the best desorption solution, sodium hydroxide (NaOH), sodium carbonate ($Na_2CO_3$), sodium chloride (NaCl), hydrochloric acid (HCl), nitric acid ($H_2NO_3$) and sulfuric acid ($H_2SO_4$) (0.1 mol $L^{-1}$) were used as scavengers for Pb(II). Dosage was 0.5 g $L^{-1}$ and the desorption time was 8 h. Besides, the reusability performance of the two materials on sodium hydroxide were conducted in-depth study with six adsorption–desorption cycles.

### 2.6 Adsorption mechanism analysis

On the basis of batch adsorption experiments, deep research on mechanism by the microstructure analysis for the samples of absorbed Pb(II) were performed which included powder X-ray diffraction (XRD), Fourier transform infrared (FT-IR), scanning electron microscopy-energy dispersive spectrometer (SEM-EDS), and X-ray photo-electron spectroscopy (XPS).

## 3. Results and discussion

### 3.1 Selection of materials

The adsorption performance of Pb(II) on different materials is shown in Fig. 1. Results revealed that $MnO_2$ had the lowest Pb(II) adsorption capacity. With initial Pb(II) concentration at 500 mg $L^{-1}$, $MnO_2$/MgFe-LDH presented superior adsorption capability compared to pure MgFe-LDH. It's worth noting that calcination temperature plays a significant role for Pb(II) removal. The higher calcination temperature for $MnO_2$/MgFe-LDH, the lower Pb(II) uptake for $MnO_2$/MgFe-LDO. Outcomes present that the adsorption capacity of Pb(II) by $MnO_2$/MgFe-$LDO_{400\ °C}$ is 496.51 mg $g^{-1}$, which is greater than $MnO_2$/MgFe-$LDO_{500\ °C}$ (417.05 mg $g^{-1}$) and $MnO_2$/MgFe-$LDO_{600\ °C}$ (354.38 mg $g^{-1}$). These phenomena could be explained by the collapse of LDH's layers at high temperature calcinations which result in a reduction in specific surface area and an irreversible memory effect. As a result, calcination temperatures of 400 °C can be the excellent candidate for calcinating $MnO_2$/MgFe-LDH to $MnO_2$/MgFe-LDO.

### 3.2 Influence of adsorbent dosage on Pb(II) adsorption

The influence results of $MnO_2$/MgFe-LDH and $MnO_2$/MgFe-$LDO_{400\ °C}$ dosages (0.5, 1.0, 1.5, 2.0, 2.5, 3.0 g $L^{-1}$) on Pb(II) (500 and 1000 mg $L^{-1}$) removal are shown in Fig. 2. As it can be seen from Fig. 2(a), a similar trend was found on the adsorption behavior in which Pb(II) removal rate enhanced from 79.15% to 99.90% for $MnO_2$/MgFe-LDH, and from 79.15% to 99.92% for $MnO_2$/MgFe-$LDO_{400\ °C}$, and then gradually tended to balance with material dosages increasing from 0.5 to 3.0 g $L^{-1}$. The subsequent increase of Pb(II) removal at a large amount of materials may result from enough adsorption sites for Pb(II)

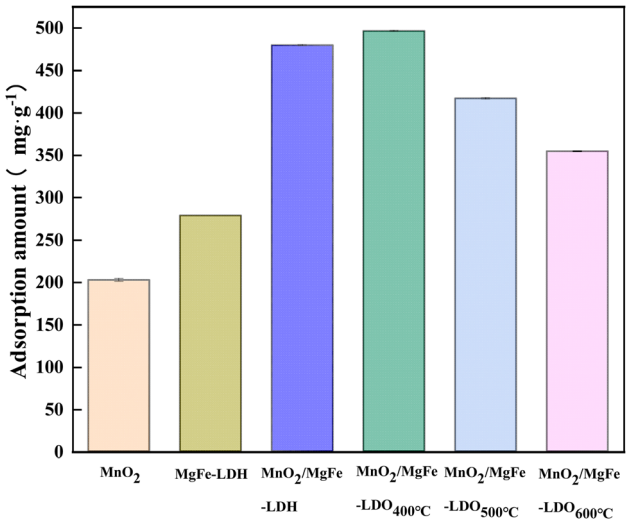


Fig. 1 Adsorption of Pb(II) on $MnO_2$, MgFe-LDH, $MnO_2$/MgFe-LDH, $MnO_2$/MgFe-$LDO_{400\ °C}$, $MnO_2$/MgFe-$LDO_{500\ °C}$, $MnO_2$/MgFe-$LDO_{600\ °C}$.

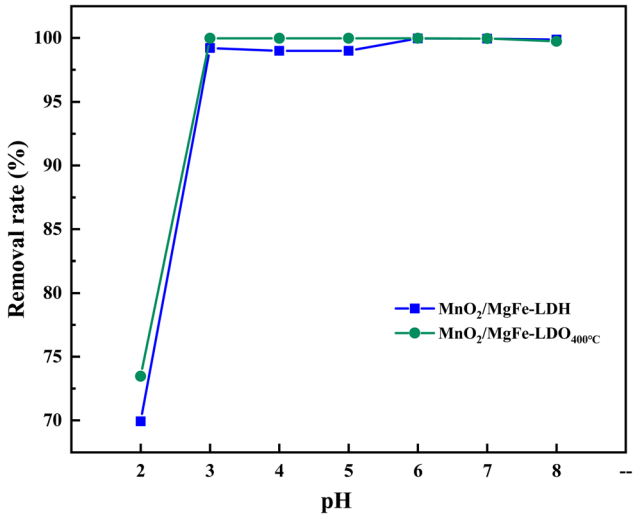


Fig. 3 The impact of pH on adsorption of Pb(II) on $MnO_2$/MgFe-LDH and $MnO_2$/MgFe-$LDO_{400\ °C}$.

when the adsorbent dosage reached 3.0 g $L^{-1}$. However, an obvious difference of Pb(II) uptake between $MnO_2$/MgFe-LDH and $MnO_2$/MgFe-$LDO_{400\ °C}$ was observed in which $MnO_2$/MgFe-$LDO_{400\ °C}$ presented a significant enhancement of Pb(II) removal with the rising dosage as can be observed in Fig. 2(b). Pb(II) removal rate could reach 65.0% when the dosage of $MnO_2$/MgFe-$LDO_{400\ °C}$ was 1.0 g $L^{-1}$. Therefore, from an economic and environmental point of view, the dosage ratio of the materials to contaminant solution, can be chosen as 1.0 g $L^{-1}$.

### 3.3 Influence of initial pH on Pb(II) adsorption

The pH value is a key factor in the adsorption process which affects not only the adsorbents' surface properties, but also the form of metal ions in solution. Hence, the adsorption performance of $MnO_2$/MgFe-LDH and $MnO_2$/MgFe-$LDO_{400\ °C}$ toward Pb(II) under various pH values were studied here, respectively. As can be seen from Fig. 3, when pH = 2.0–3.0, LDH and LDO still have a high removal rate of Pb in extremely acidic environment, which is more than 70%.[39] Once the pH values greater than 3.0, adsorption efficiency kept nearly stable, with the high removal efficiency of 99.97% on the two composite adsorbents. While, it is worth noting that $MnO_2$/MgFe-$LDO_{400\ °C}$ ($pH_{zpc}$ = 5.40) exhibited a positive charged surface at pH = 3.0–5.4, as evidenced by zeta-potential results in our previous research.[30] Similar results were observed for Pb(II) removal by $MnO_2$/MgFe-LDH. That is, $MnO_2$/MgFe-LDH and $MnO_2$/MgFe-$LDO_{400\ °C}$ should be inhibited Pb(II) removal because of electrostatic repulsion. However, the removal rate of Pb(II) was still high in the pH range of 3.0–5.0, illustrating that the other interaction should occur between Pb(II) and adsorbents. It is supposed that LDH or LDO could release $OH^-$ during the hydration, subsequently precipitating with lead ion in the solution.[40] Moreover, the loaded $MnO_2$ on LDO may be another reason for the high removal efficiency of Pb(II) in a wide pH range.

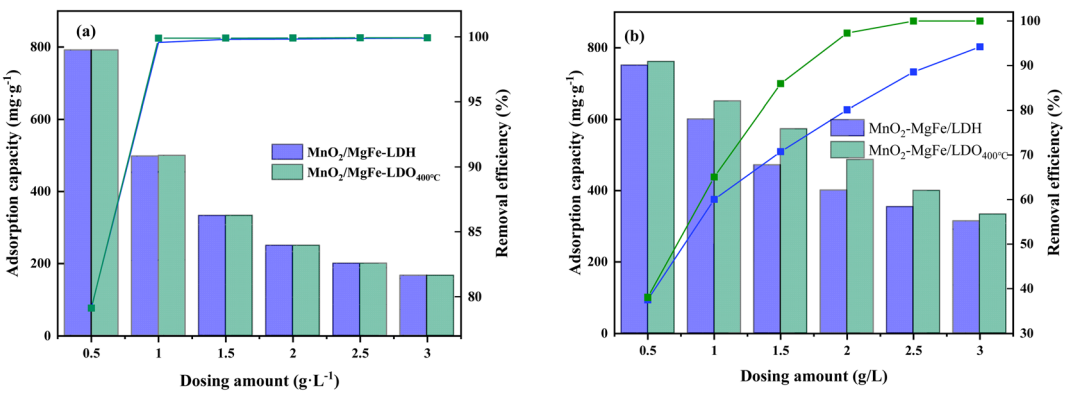


Fig. 2 The influence of dosage on adsorption of Pb(II) on $MnO_2$/MgFe-LDH and $MnO_2$/MgFe-$LDO_{400\ °C}$: (a) Pb(II) 500 mg $L^{-1}$; (b) Pb(II) 1000 mg $L^{-1}$.

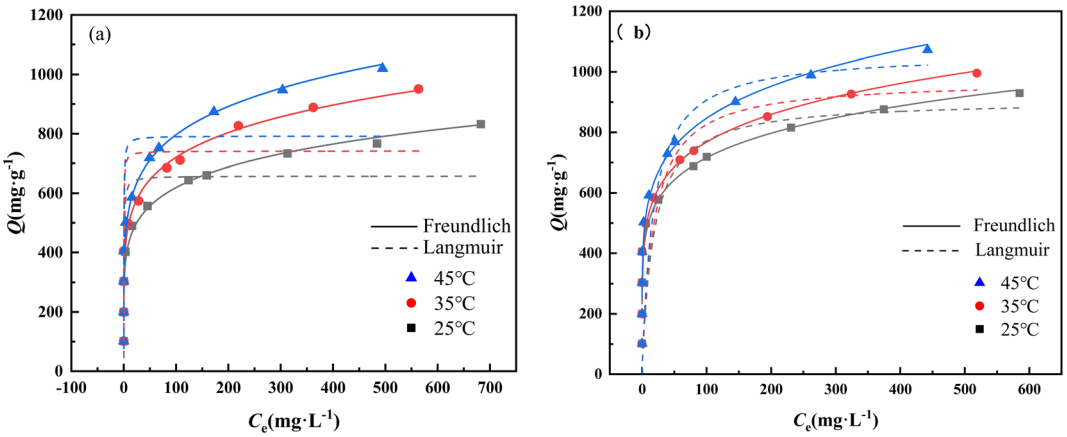


Fig. 4 Isothermal adsorption models of two composites for Pb(II) adsorption: (a) isothermal model for $MnO_2$/MgFe-LDH adsorption; (b) isothermal model for $MnO_2$/MgFe-$LDO_{400\ °C}$ adsorption.

### 3.4 Influences of the initial concentration and isotherms

To evaluate the adsorption behavior of $MnO_2$/MgFe-LDH and $MnO_2$/MgFe-$LDO_{400\ °C}$ at different Pb(II) concentrations, the effect of initial concentration of Pb(II) was investigated over a concentration of 100–1500 mg $L^{-1}$ at three different temperatures, which the results are presented in Fig. 4. Obviously, the adsorption capacity increases significantly with the initial concentration rising at the same temperature resulting from the enhancement in the numbers of lead ions available for chelating with the binding sites of adsorbents. Besides, an increase in the adsorption capacity of Pb(II) with the increase of temperature at the same initial concentration, indicating that the adsorption processes of Pb(II) by $MnO_2$/MgFe-LDH and $MnO_2$/MgFe-$LDO_{400\ °C}$ were an endothermic reaction, these results are also consistent with the findings of Md. Tofazzal Hossain.[41] The increase in temperature causes the solute molecules in the system to move faster, increasing the mass transfer rate and diffusion coefficient, and thus increasing the adsorption capacity. Furthermore, two typical adsorption isotherm models, Langmuir and Freundlich, have been applied to the adsorption data by two composites. The Langmuir model can be employed to depict the homogeneous adsorption process, where in all sites contained on a finite number of homogeneous surfaces have an equal affinity for the adsorbate.[24,42,43] The Freundlich model can be employed to illustrate the heterogeneous adsorption process, where the adsorbate molecules interact with each other. It is in connection with physical interaction.[33,43] The obtained results are listed in Table 1. Comparing the correlation coefficients $R^2$ of the two models, Freundlich isothermal adsorption model was better for description of equilibrium data which implies that multilayer adsorption of Pb(II) by $MnO_2$/MgFe-LDH and $MnO_2$/MgFe-$LDO_{400\ °C}$ was the predominant reaction. In addition, $0.1 < 1/n < 0.2$ in the Freundlich model suggested that the adsorption of Pb(II) is easy to proceed with a strong force between the adsorbent and the metal ions.[33] The maximum monolayer adsorption capacity of $MnO_2$/MgFe-$LDO_{400\ °C}$ on Pb(II) adsorption from Langmuir isotherm was 1062.80 mg $L^{-1}$ of which was the best compared with adsorption capacity of other LDH or LDO based materials as listed in Table 2. The adsorption capability of $MnO_2$/MgFe-LDH and $MnO_2$/MgFe-$LDO_{400\ °C}$ for Pb(II) significantly exceeded that of other composite materials in the literatures.[23,24,42,44–48]

### 3.5 Influences of adsorption time and kinetics

Three common kinetic models including the pseudo-first-order kinetic model, pseudo-second-order kinetic model, and Elovich mode are used to understand the nature of the adsorption which the results are show in Fig. 5 and related parameter are listed in Table 3. As shown in Table 3, the correlation coefficients $R^2$ of the two composites at two different concentrations, both of $MnO_2$/MgFe-LDH ($R^2 > 0.998$) and $MnO_2$/MgFe-$LDO_{400}$ ◦

Table 1 Parameters of adsorption isotherm model

| | | Langmuir model | | | Freundlich model | | |
|---|---|---|---|---|---|---|---|
| Materials | Temperature | $q_m$ (mg $g^{-1}$) | $K_L$ | $R^2$ | $K_F$ | $1/n$ | $R^2$ |
| $MnO_2$/MgFe-LDH | 25 °C | 657.91 | 2.091 | 0.776 | 306.316 | 0.153 | 0.975 |
| | 35 °C | 741.38 | 3.883 | 0.773 | 348.159 | 0.158 | 0.952 |
| | 45 °C | 791.96 | 3.105 | 0.780 | 375.254 | 0.163 | 0.961 |
| $MnO_2$/MgFe-$LDO_{400\ °C}$ | 25 °C | 907.10 | 0.057 | 0.785 | 350.542 | 0.155 | 0.948 |
| | 35 °C | 971.74 | 0.056 | 0.809 | 362.648 | 0.163 | 0.950 |
| | 45 °C | 1062.80 | 0.058 | 0.831 | 386.458 | 0.170 | 0.954 |

Table 2 Comparison of Pb(II) removal with other reported adsorbents

| Adsorbents | $C_0$ (mg $L^{-1}$) | Adsorption capacities (mg $g^{-1}$) | Ref. |
|---|---|---|---|
| CS-LDH | 300 | 333.3 | 23 |
| Magnetic graphene oxide/MgAl-LDH | 300 | 192.3 | 24 |
| ZnAl@BC-LDH | 500 | 285.2 | 39 |
| Ni–Fe–$CO_3$ LDH-NGO | 1000 | 986.5 | 40 |
| CoMo($CO_3$) LDH | 370 | 73.4 | 41 |
| G/S-LDO | 1400 | 720.1 | 42 |
| N–Co@C/NiCo-LDO | 800 | 427.4 | 43 |
| Mag-LDO/C | 400 | 359.7 | 44 |
| $MnO_2$/MgFe-LDH | 1000 | 791.9 | This study |
| $MnO_2$/MgFe-LDO$_{400\ ^\circ C}$ | 1000 | 1062.8 | This study |

$_C$ ($R^2 > 0.999$) are more consistent with the pseudo-second-order kinetic model which have higher $R^2$ values than that of pseudo-first-order kinetic. Besides, the equilibrium adsorption capacities of Pb(II) and obtained from pseudo-second-order kinetic model at three concentrations were well in agreement together reflecting the better description of experimental kinetic data with this model. The fitting equilibrium adsorption capacities obtained for $MnO_2$/MgFe-LDH at two concentrations were 684.93, and 775.19 mg $g^{-1}$. Similarly, the equilibrium adsorption capacities of Pb(II) by $MnO_2$/MgFe-LDO$_{400\ ^\circ C}$ at two concentrations were 735.29, and 840.31 mg $g^{-1}$, which were higher than that of $MnO_2$/MgFe-LDH. Considering the formation of chemical bonds is the main factor affecting the pseudo-second-order kinetic adsorption, $MnO_2$ loading and calcination endowed $MnO_2$/MgFe-LDO$_{400\ ^\circ C}$ with strong affinity with Pb(II) by chemisorption should be a promising material applied in wastewater treatment.[24]

In addition, to reveal heterogeneous diffusion controlled by reaction rate and diffusion, the Elovich model (eqn (5)) was also employed to understand the kinetics of adsorption behavior on $MnO_2$/MgFe-LDH and $MnO_2$/ MgFe-LDO$_{400\ ^\circ C}$ composite. As shown in Table 3, the removal process of Pb(II) by $MnO_2$/MgFe-LDH and $MnO_2$/MgFe-LDO$_{400\ ^\circ C}$ was matched with the Elovich model well ($R^2 > 0.950$), revealing heterogeneous diffusion occurred including film diffusion and ion diffusion in the micro adsorbent pore.[42,43]

### 3.6 Adsorption thermodynamics

Thermodynamics was studied to gain more insights into the adsorption mechanism of Pb(II) on $MnO_2$/MgFe-LDH and $MnO_2$/MgFe-LDO$_{400\ ^\circ C}$. It reveals spontaneity and equilibrium of adsorption through parameters like enthalpy change ($\Delta H$, kJ $mol^{-1}$), Gibbs free energy ($\Delta G$, kJ $mol^{-1}$) and entropy change ($\Delta S$, J $mol^{-1}$ $K^{-1}$). The results are shown in Fig. 6 by using $1/T$ as horizontal and $\ln K_e$ as vertical coordinates for the graphs respectively. And the relatively thermodynamical parameters are presented in Table 4. As can be seen from Table 4, the $\Delta G^0$ of Pb(II) adsorption by $MnO_2$/MgFe-LDH and $MnO_2$/MgFe-LDO$_{400\ ^\circ C}$ at 25, 35, and 45 °C were all negative (−2.1299, −3.2249, −4.3199; −3.1049, −3.9572, −4.8102 kJ $mol^{-1}$), indicating that the adsorption for two composites on Pb(II) uptake was a spontaneous reaction.[49] The positive values of $\Delta H^0$ (30.5175, 22.3304 kJ $mol^{-1}$) reflect that the adsorption process is an endothermic process involving chemisorption. Besides, $\Delta S^0$ value is positive (109.50 J $mol^{-1}$ $K^{-1}$ for $MnO_2$/MgFe-LDH, 85.31 J $mol^{-1}$ $K^{-1}$ for $MnO_2$/MgFe-LDO$_{400\ ^\circ C}$) which indicated that good affinity of the $MnO_2$/MgFe-LDH and $MnO_2$/MgFe-LDO$_{400\ ^\circ C}$ with Pb(II) and showed an increase in the degree of freedom of the adsorbed species.[50]

### 3.7 Repeated regeneration experiments of materials

Different chemicals of NaOH, $Na_2CO_3$, NaCl, HCl, $HNO_3$, and $H_2SO_4$ with an initial concentration of 0.1 mol $L^{-1}$ were selected as Pb(II) dissolvers to explore the recycling performance of the materials on Pb(II). As shown in Fig. 7(a), the adsorption properties of $MnO_2$/MgFe-LDH and $MnO_2$/MgFe-LDO$_{400\ ^\circ C}$ on Pb(II) exhibited distinct differences after desorption by different solvents. It is worth noting the material of $MnO_2$/MgFe-LDO$_{400\ ^\circ C}$ still presents a high adsorption performance of Pb(II) (473.41 mg $L^{-1}$) after desorbed by NaOH, illustrating that NaOH was the most suitable desorption agent here. Previous literatures have shown that NaOH solution is available for the desorption of precipitated carbonate/lead hydroxide from materials. For example, Emmanuel Abu-Danso's[51] research showed that 0.1 M NaOH is a better eluent for the regeneration of CNFs. Waqas Ahmed[52] was also used NaOH as elution agent to remove lead from a red mud modified rice-straw biochar. According to our experimental results, the elution performance of NaOH is the best among the six elutes. Therefore, NaOH was selected as the eluent for the cyclic experiment.

We select 0.1 mol $L^{-1}$ NaOH as the dissolver to study the influence of the number of adsorption–desorption process on Pb(II) adsorption capacity for the two composites. It can be seen from Fig. 7(b) that the Pb(II) adsorption capacity on two composites decreased with the increase of the number of adsorption–desorption, and the adsorption capacity of $MnO_2$/MgFe-LDH decreased from 356.30 mg $g^{-1}$ in the first recycling to 6.20 mg $g^{-1}$ in the sixth recycling round, and the adsorption capacity of Pb(II) of $MnO_2$/MgFe-LDO$_{400\ ^\circ C}$ decreased from 473.69 mg $g^{-1}$ to 16.87 mg $g^{-1}$ similarly. In general, the Pb(II) removal performance of $MnO_2$/MgFe-LDO$_{400\ ^\circ C}$ is better than that of $MnO_2$/MgFe-LDH during the recycling experiments. Combined with $K_{sp}$ ($Pb(OH)_2$) = $1.2 \times 10^{-15}$ < $K_{sp}$ ($Pb(CO_3)_2$) = $7.4 \times 10^{-14}$, the higher desorption of Pb(II) occurring on $MnO_2$/

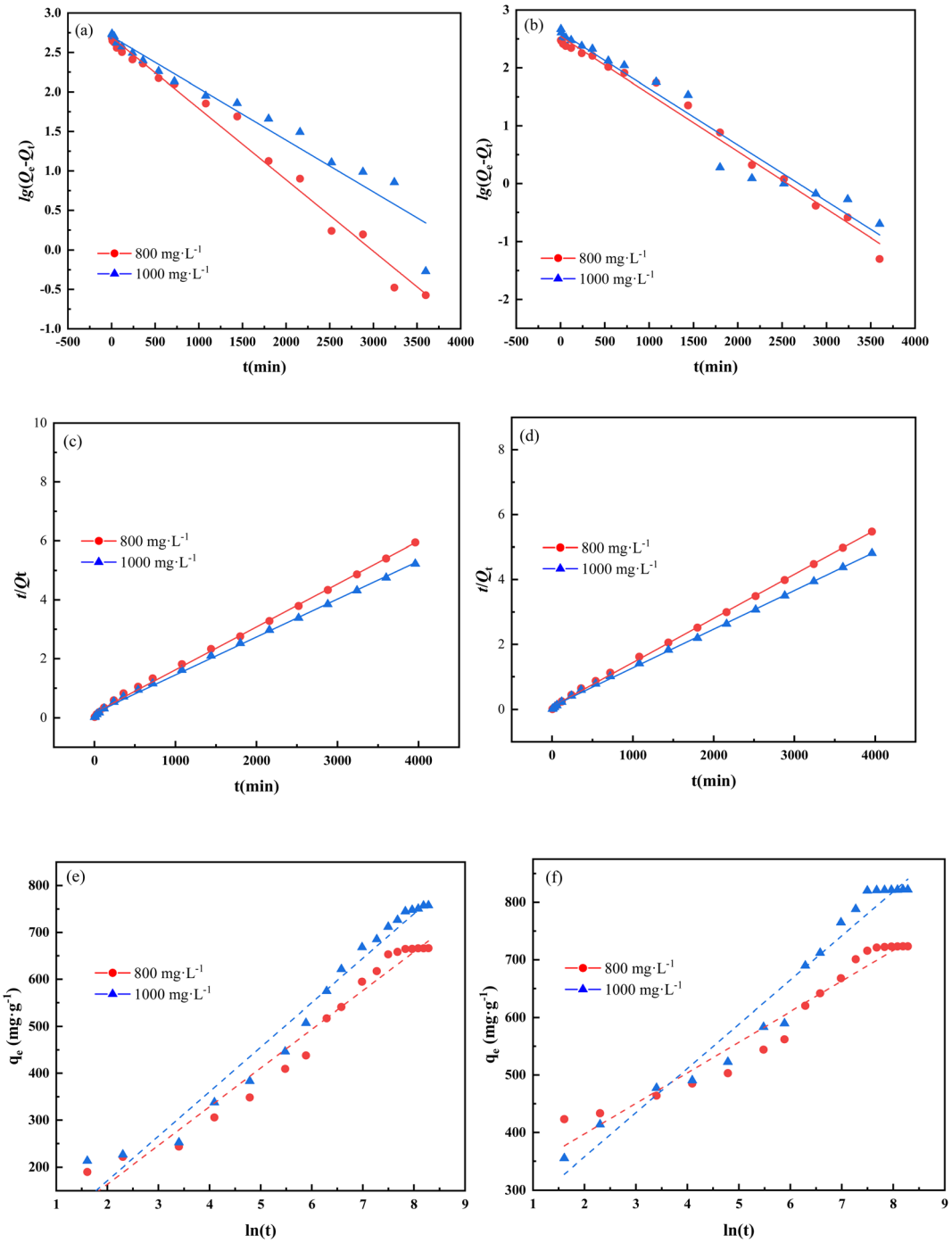


Fig. 5 Kinetic model (a) and (b) quasi-primary kinetic model of $MnO_2$/MgFe-LDH and $MnO_2$/MgFe-$LDO_{400\ °C}$; (c) and (d) quasi-secondary kinetic model of $MnO_2$/MgFe-LDH and $MnO_2$/MgFe-$LDO_{400\ °C}$; (e) and (f) Elovich model of $MnO_2$/MgFe-LDH and $MnO_2$/MgFe-$LDO_{400\ °C}$.

MgFe-LDH and $MnO_2$/MgFe-$LDO_{400\ °C}$ might be attributed to the reaction of surface co-precipitation between absorbed Pb(II) and NaOH by the following equation.

$$n Pb_3(CO_3)_2(OH)_2 + 2(n+2)NaOH = (n+1)Na_2[Pb(OH)_4] + Na_2CO_3 \quad (12)$$

However, it's worth noting that this process may not affect the chemical structure of the materials.[33]

Although the adsorption performance of our material degrades with the number of cycles, LDHs nanoparticles are simple to manufacture, inexpensive, and both manganese dioxide and LDHs are derived from environmental soil, making them ecologically acceptable materials. In terms of comprehensive material properties, economic and environmental benefits, LDHs/LDOs can be used as a good lead adsorbent.

Table 3 Kinetic model parameters

| | | Quasi-primary kinetic model | | | Quasi-secondary kinetic model | | | Elovich model | | |
|---|---|---|---|---|---|---|---|---|---|---|
| Materials | $C_0$ (mg $L^{-1}$) | $Q_e$ (mg $g^{-1}$) | $K_1$ | $R^2$ | $Q_e$ (mg $g^{-1}$) | $K_1$ | $R^2$ | $\alpha$ | $\beta$ | $R^2$ |
| $MnO_2$/MgFe-LDH | 800 | 494.31 | $9.034 \times 10^{-4}$ | 0.986 | 684.93 | $1.252 \times 10^{-5}$ | 0.998 | 81.266 | 0.012 | 0.967 |
| | 1000 | 504.61 | $6.565 \times 10^{-4}$ | 0.944 | 775.19 | $1.054 \times 10^{-5}$ | 0.998 | 78.057 | 0.011 | 0.969 |
| $MnO_2$/MgFe-LDO | 800 | 350.53 | $9.942 \times 10^{-4}$ | 0.988 | 735.29 | $2.387 \times 10^{-5}$ | 0.999 | $1.27 \times 10^{4}$ | 0.019 | 0.950 |
| | 1000 | 410.63 | $9.727 \times 10^{-4}$ | 0.964 | 840.34 | $2.755 \times 10^{-5}$ | 0.999 | $1.09 \times 10^{3}$ | 0.013 | 0.963 |

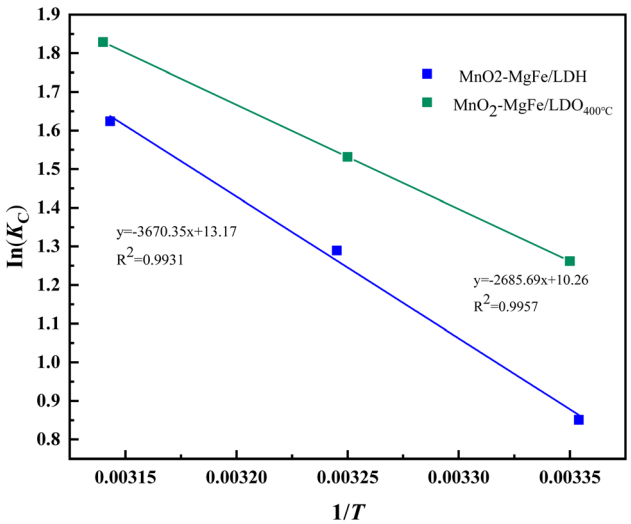


Fig. 6 Adsorption thermodynamics of Pb(II) on $MnO_2$/MgFe-LDH and $MnO_2$/MgFe-$LDO_{400\ °C}$.

# 4. Mechanism discussion

A series of characterizations had been carried out to further elucidate the interaction mechanisms between $MnO_2$/MgFe-LDH or $MnO_2$/MgFe-$LDO_{400\ °C}$ and Pb(II) after the adsorption performance. The raw materials of $MnO_2$/MgFe-LDH or $MnO_2$/MgFe-$LDO_{400\ °C}$ have been characterized in our previous study.[30] These characterizations were mainly including X-ray diffraction (XRD), Fourier transform infrared spectroscopy (FT-IR), scanning electron microscopy (SEM), transmission electron microscopy (TEM), and X-ray photoelectron spectroscopy (XPS).

## 4.1 Precipitating action

The previous research proved that the precipitation is an important removal reaction between materials and the heavy metals because some anions (such as $CO_3^{2-}$, $OH^-$) could be released from LDH/LDO during the adsorption process.[33,34,44] Compared to our previous research,[30] the spectrum of $MnO_2$/

Table 4 Parameters of adsorption thermodynamics of Pb(II) on $MnO_2$/MgFe-LDH and $MnO_2$/MgFe-$LDO_{400\ °C}$

| Materials | Temperature (°C) | $\Delta G^0$ (kJ $mol^{-1}$) | $\Delta S^0$ [J $(mol\ K)^{-1}$] | $\Delta H^0$ (kJ $mol^{-1}$) |
|---|---|---|---|---|
| $MnO_2$/MgFe-LDH | 25 | −2.1299 | 109.50 | 30.5175 |
| | 35 | −3.2249 | | |
| | 45 | −4.3199 | | |
| $MnO_2$/MgFe-$LDO_{400\ °C}$ | 25 | −3.1049 | 85.31 | 22.3304 |
| | 35 | −3.9572 | | |
| | 45 | −4.8102 | | |

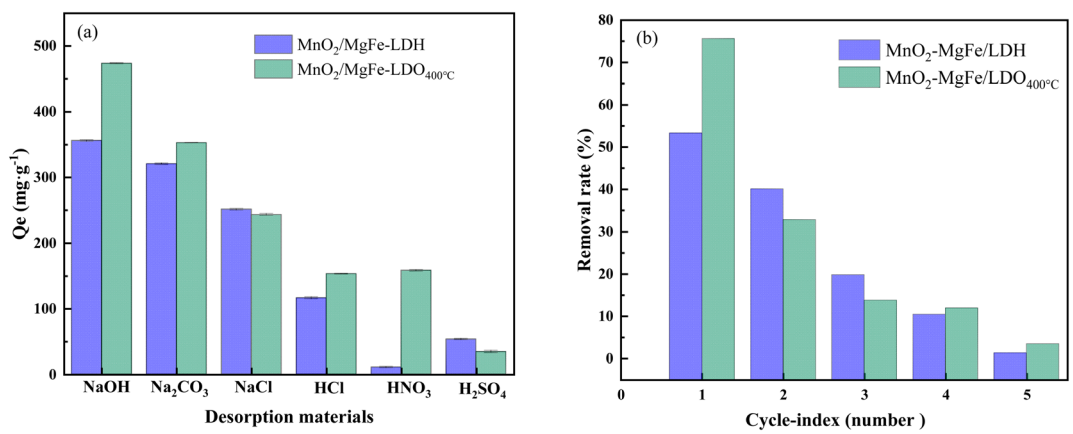


Fig. 7 (a) Six analytical agents on the desorption effect of Pb(II) (b) repeated regeneration performance of $MnO_2$/MgFe-LDH and $MnO_2$/MgFe-$LDO_{400\ °C}$ materials.

MgFe-LDH showed typical peaks of the (0 0 3), (0 0 6), (0 1 2), (0 1 5), and (1 1 0) planes which belonging to the LDH material. The existence peaks of the (0 1 2) and (1 1 0) planes confirmed the hexagonal lattice, that is attributed to the stretching mode of $CO_3^{2-}$ present in between $MnO_2$/MgFe-LDH.[53] Fig. 8(a) illustrates the new diffraction peaks also appeared at $2\theta = 19.855°$ (101), 20.885° (012), 24.638° (104), 27.148° (015), 32.964° (107), 34.143° (110), 36.026° (113), 40.396° (202), 42.585° (024), 43.029° (1010), 44.233° (205), 48.222° (027), 48.956° (119), 54.014° (122), 58.195° (0114), 60.459° (217) after the adsorption of Pb(II) by $MnO_2$/MgFe-LDH and $MnO_2$/MgFe-LDO$_{400\ °C}$, which are in high agreement with the $Pb_3(CO_3)_2(OH)_2$ standard card PDF#96-901-1389.[54]

By comparing the surface morphology of $MnO_2$/MgFe-LDH and $MnO_2$/MgFe-LDO$_{400\ °C}$ after Pb(II) adsorption (shown in Fig. 9(a1), (a2), (b1) and (b2)), a typical arrangement of hydrotalc like sheet structure and stacked precipitant was observed on the surface of these two samples which is indicative of the precipitation presence. From the XPS results shown in Fig. 10(a), new peaks belonging to Pb 4f observed after adsorption of Pb(II) by $MnO_2$/MgFe-LDH and $MnO_2$/MgFe-LDO$_{400\ °C}$. Besides, Fig. 10(b) and (c) present that the Pb $4f_{5/2}$ was also observed at the binding energy of 144.51 eV and 143.06 eV corresponding to the Pb(II) oxidation state which confirmed the emergence of $Pb_3(CO_3)_2(OH)_2$.[23]

Therefore, Pb(II) adsorption on the two materials mainly resulted from surface coprecipitation among Pb(II), interlayer $CO_3^{2-}$ and interlayer $OH^-$ of hydrotalcite as described by the following equations.[33]

$$3Pb^{2+} + CO_3^{2-} + 4OH^- \rightarrow PbCO_3 + 2Pb(OH)_2 \rightarrow Pb_3(CO_3)_2(OH)_2\downarrow \quad (13)$$

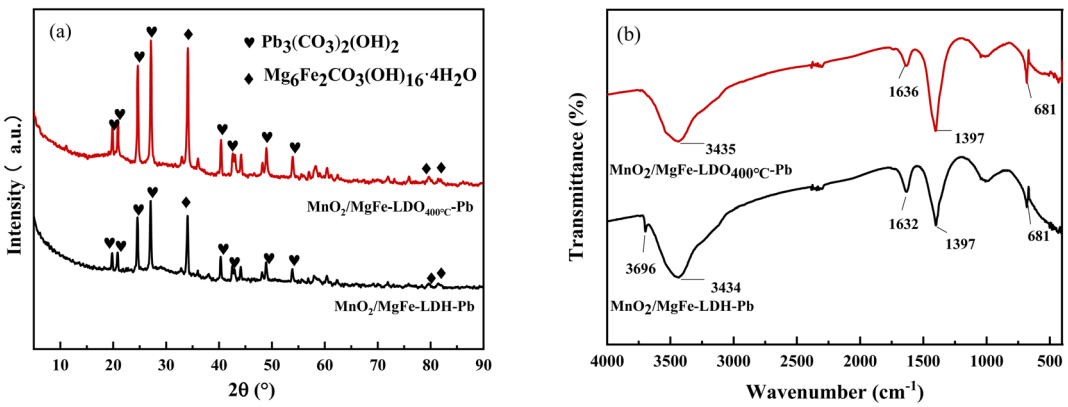


Fig. 8 (a) XRD spectra of materials after Pb(II) adsorption; (b) FTIR spectra of materials after Pb(II) adsorption.

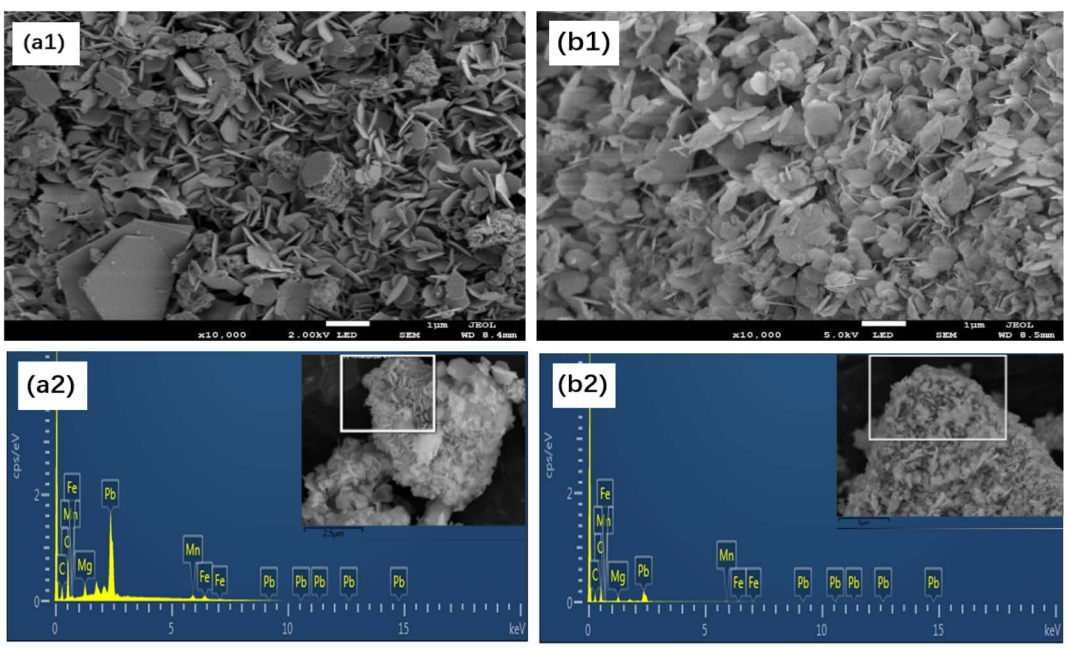


Fig. 9 SEM images of (a1) $MnO_2$/MgFe-LDH and (b1) $MnO_2$/MgFe-LDO$_{400\ °C}$ after Pb(II) adsorption; EDS spectrum of (a2) $MnO_2$/MgFe-LDH, (b2) $MnO_2$/MgFe-LDO$_{400\ °C}$ after Pb(II) adsorption.

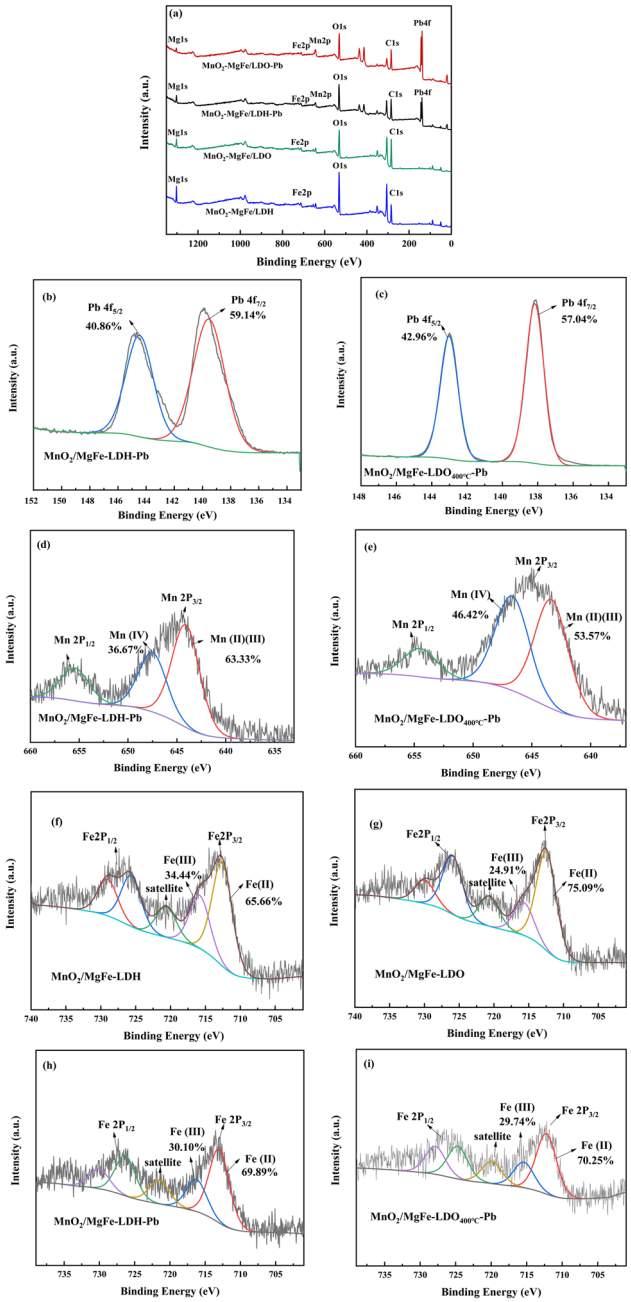


Fig. 10 (a) XPS survey; (b) and (c) Pb 4f spectrums of $MnO_2$/MgFe-LDH and $MnO_2$/MgFe-$LDO_{400\ °C}$ after reaction; (d) and (e) Mn2p spectrums of $MnO_2$/MgFe-LDH and $MnO_2$/MgFe-$LDO_{400\ °C}$ after reaction (plot of Mn 2p spectrums before reaction is in our previous study[28]); (f) and (g) Fe spectrums of $MnO_2$/MgFe-LDH and $MnO_2$/MgFe-$LDO_{400\ °C}$ before reaction; (h) and (i) Fe spectrums of $MnO_2$/MgFe-LDH and $MnO_2$/MgFe-$LDO_{400\ °C}$ after reaction.

### 4.2 Complexation with functional groups

In general, the oxygen-containing functional groups (OFGs) could chelate with heavy metals in aqueous solution and it showed great significance in removing contaminants from water.[55] The surface complexation may be mainly and rapidly due to the large specific surface area and surface functional groups of the $MnO_2$/MgFe-LDH and $MnO_2$/MgFe-LDO.

According to FTIR measurements, Fig. 8(b) displayed that the peaks at 3696 and 3434 $cm^{-1}$ after Pb(II) adsorption are weaker than those before the adsorption.[56] Moreover, the peaks at 1386 $cm^{-1}$ for $MnO_2$/MgFe-LDH and 1440 $cm^{-1}$ for $MnO_2$/MgFe-$LDO_{400\ °C}$ caused by the bending vibration of O–H which showed a shift to 1397 $cm^{-1}$ after the adsorption, indicating that the Pb(II) removal process occurred by complexation with functional groups to generate $Pb(OH)_2$.[45,53] The new absorption peak with a wave number of 681 $cm^{-1}$ belongs to metal oxygen and is identified as Pb–O.[57] The absence of absorption peaks in the low-frequency region (less than 1000 $cm^{-1}$) are caused by O–M or O–M–O (M = Fe, Mn) bending vibrations, suggested that Mn–O, Fe–O, O–Mn–O, O–Fe–O were engaged in the complexation reaction that removed Pb(II).[58,59]

To further confirm the roles of Mn species on $MnO_2$/MgFe-LDH, $MnO_2$/MgFe-$LDO_{400\ °C}$, we have also analyzed the Mn elemental changes (Fig. 10(d) and (e)). The main peak of the Mn 2p doublet is shifted to a higher binding energy, so we confirmed that Mn is involved in the chemical reaction.[25] Compared to our previous study,[30] $MnO_2$/MgFe-LDH's relative proportion of Mn(II)/Mn(III) increased from 49.38% to 63.33% after the reaction. For $MnO_2$/MgFe-$LDO_{400\ °C}$, the relative proportion of Mn(II)/Mn(III) increased from 51.10% to 53.57%. These results suggest the reduction of Mn(IV) to Mn(II), indicating that Mn(IV) participates in electron transfer, means Mn–O on the surface participated in the reaction.[59]

Meanwhile, before adsorption, $MnO_2$/MgFe-LDH and $MnO_2$/MgFe-$LDO_{400\ °C}$ had the Fe 2p peaks which are centered at the binding energies of 711.87–711.97 eV, with the typical values for Fe(III) in Fe(OH)O[60] (Fig. 10(f) and (g)). The fraction of Fe(II) in $MnO_2$/MgFe-LDH increases from 65.66% to 69.89% and the fraction of Fe(II) in $MnO_2$/MgFe-$LDO_{400\ °C}$ decreased from 75.09% to 70.25% (Fig. 10(h) and (i)). These are due to the presence of large amounts of Fe(II) in the calcined LDO, being replaced by the Fe(III) after placed in water. This explains the better adsorption performance of LDO. Overall, self-oxidation-reduction reaction occurred during the testing process.[57] Besides, according to EDS results, the quality fraction of Fe in LDO increase, therefore, the superiority of LDO adsorption over LDH may be due to an increase in oxygen-containing functional groups or to a memory effect.

In addition, it was obvious that the peaks of Pb 4f appeared after adsorption, and both can befit individually into two sub-peaks. This result is similar to Lingmin Sun's research,[50] which confirmed the surface adsorption of Pb(II) by both $MnO_2$/MgFe-LDH, $MnO_2$/MgFe-$LDO_{400\ °C}$. From the Fig. 10(b)–(c), the Pb $4f_{5/2}$ and Pb $4f_{7/2}$ indicated the formation of complexations, such as Sur-OH-$Pb^{2+}$, Sur-O-$Pb^{2+}$, or Sur-COO-$Pb^{2+}$ (Sur means deprotonation).[24]

### 4.3 Electrostatic attraction

According to previous research,[30] $MnO_2$/MgFe-LDO ($pH_{zpc}$ = 5.40) exhibits a higher positive charge than $MnO_2$/MgFe-LDH ($pH_{zpc}$ = 4.95). It shows a stronger electrostatic repulsion for the cation Pb(II), which is not conducive to the adsorption of Pb(II) by the material. However, $MnO_2$/MgFe-LDO material exhibits better

adsorption performance for Pb(II) within the pH range of 2.0–5.0. These phenomena contributed to the anions such as $CO_3^{2-}$ and $OH^-$ are released between the layers of the composites which will gradually increase the pH of the solution. When the solution pH value was larger than 5.4, the two materials carried stronger positive charge on their surface and had a stronger affinity for Pb(II). As a result, both composites have a negative surface charge and an electrostatic gravitational force between them and Pb(II), facilitating the adsorption.[39] It illustrates that electrostatic adsorption may exist in the Pb(II) adsorption process.

### 4.4 Cation exchange and isomorphic replacement

It is easy for the $MnO_2$/MgFe-LDH to combine with heavy metals because of the exchangeable ions existence. The interactions occurred also simultaneously during the adsorption process. Generally, isomorphic substitution of the LDH occurs by the element's replacement in the LDH crystal structure. The total ionic charge and size of the substitutional atoms or ions must be the identical or similar to those of the atoms of the LDH.[61] The atoms ratios of $M^{2+}/M^{3+}$ in $MnO_2$/MgFe-LDH and $MnO_2$/MgFe-LDO before and after adsorption can be calculated using the XPS data.[24] According to XPS results, after Pb(II) was adsorbed, the $Mg^{2+}/Fe^{3+}$ atomic ratio of the $MnO_2$/MgFe-LDH (2.64) and $MnO_2$/MgFe-LDO (1.93) decreased to 1.57 and 1.12, respectively. This was attributed to the isomorphic replacement of $Mg^{2+}$ in the $MnO_2$/MgFe-LDH and $MnO_2$/MgFe-LDO by the metal ions and $Mg^{2+}$ moving into the solution. Therefore, incorporating the Pb(II) by the substitution of $Mg^{2+}$ ions into the LDH.

### 4.5 Memory effect

The LDO is formed by heating the LDHs. As the heating temperature rises, the LDHs bilayers of adsorbed water and interlayer crystalline water are gradually evaporated. The reason why LDO has better adsorption property: firstly, the memory effect of LDO is due to transition of its disordered layered structure into ordered layered structure, LDO transforms into LDH. Secondly, LDH would slightly release $Mg^{2+}$ and $OH^-$ which would raise the pH of micro-environment around the LDH surface.[62] Thirdly, some Pb ions enter the LDH skeleton, take over the Mg position and forms MgPbFe-LDH by the cation-exchange mechanism; concomitantly, some Pb ions form precipitates with $OH^-$ as base or basic salt. Consequently, Pb ions are separated from the aqueous solution. Therefore, the cooperative effect of cation exchange and deposition makes our $MnO_2$/MgFe-LDO highly efficient in up-taking Pb ions. The X-ray diffraction patterns of the LDO also demonstrate that the adsorption is significantly enhanced by the reconstruction of its original layered structure in the presence of lead with the memory effect.[63] According to BET results,[30] the roasted $MnO_2$/MgFe-LDO has a larger specific surface area and a more developed pore structure, which makes it easier for adsorption or better for the "memory effect" to promote the chemical precipitation of Pb(II). Therefore, LDO has better adsorption performance than LDH.[64]

In summary, the adsorption experiment combined with XRD, FT-IR, SEM-EDS, and XPS, to present the adsorption mechanisms of Pb(II) on the two composites were summarized in Fig. 11 which mainly included: (1) precipitating action as shown in Fig. 11(a): as the reaction proceeds, the increased concentration of Pb(II) around the two composites reacts with the anions such as $CO_3^{2-}$ and $OH^-$ released between the layers on the adsorbent surface. (2) Complexation with functional groups as shown in Fig. 11(b): Pb(II) is locked to the surface of the material by reacting with oxygen-containing groups on the surface of both composites, such as Mn–O, Fe–O to produce

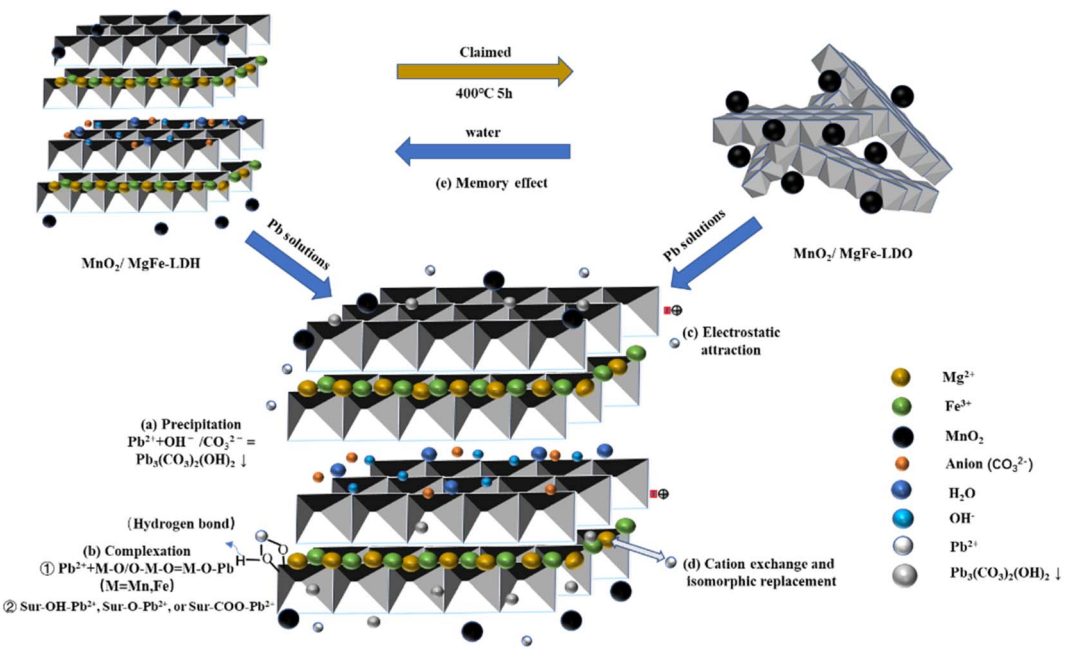


Fig. 11 The Pb(II) adsorption mechanism of $MnO_2$/MgFe-LDH and $MnO_2$/MgFe-$LDO_{400\ ^\circ C}$.

Mn/Fe–O–Pb; (3) electrostatic attraction as shown in Fig. 11(c): anions such as $CO_3^{2-}$ and $OH^-$ are released between the composite layers and the solution pH gradually increases. The surface of both composites is negatively charged and electrostatic gravitational forces exist between them and Pb(II). (4) Cation exchange and isomorphic replacement as shown in Fig. 11(d): incorporation of Pb(II) into LDH by substitution of $Mg^{2+}$ ions. (5) Memory effect as shown in Fig. 11(e): with a larger specific surface area and more developed pore structure, $MnO_2$/MgFe-LDO undergoes reconstruction after being placed in water, during which a large amount of $OH^-$ is generated.

## 5. Conclusions

This study aimed to obtain $MnO_2$/MgFe-LDH and $MnO_2$/MgFe-LDO materials with improved properties toward the removal of Pb(II) ions by adjusting some of the synthesis parameters (*i.e.*, calcined temperature and aging time). The results showed that ternary layered structure-like hydrates with high crystallinity and tiny particle size can be prepared by co-precipitation. During calcination, the characteristic peaks, crystal image, surface roughness, pore size, and volume of the material become more evident. Thus, an increased number of adsorption sites and more active groups are active between layers.

Results suggest that $MnO_2$/MgFe-LDO$_{400\ ^\circ C}$ has better adsorption performance on Pb(II), the pseudo-second-order kinetic model and Freundlich isothermal adsorption model are better compatible with the adsorption process of $MnO_2$/MgFe-LDO$_{400\ ^\circ C}$ on Pb(II). The adsorption mechanisms of Pb(II) on the two composites are mainly complexation, complexation with functional groups, electrostatic interaction, cation exchange and isomorphic replacement, as well as memory effect for $MnO_2$/MgFe-LDO$_{400\ ^\circ C}$.

## Author contributions

L. C. M. and Y. S. H.: the corresponding author had studied the property of the prepared material besides sharing in manuscript writing and in the experimental design, methodology preparation, statistical analysis, discussion, figures plotting, and follow-up experimental details. H. Y. X., L. X. P., Saeed R., Q. L. T.: shared in the experimental design, methodology preparation, characterization, statistical analysis, discussion, figures plotting, follow-up experimental details, collecting the experimental data, revised the manuscript in its final form before submission and helped in discussion modifications.

## Conflicts of interest

The authors declare that they have no known competing financial interests or personal relationships that could have appeared to influence the work reported in this paper.

## Acknowledgements

This research was funded by the Science & Technology Program of Guangxi (Grant No. Guike AD19110007), the Research Funds of The Guangxi Key Laboratory of Theory and Technology for Environmental Pollution Control (Grant No. Guikeneng 1801K010), Research Foundation of Guilin University of Technology (Grant No. GUTQDJJ201808).

## References

1 R. Zhang, V. L. Wilson, A. X. Hou and G. Meng, *International Journal Of Health, Animal Science And Food Safety*, 2015, **2**, 18–31.
2 K. G. Sreejalekshmi, K. A. Krishnan and T. Anirudhan, *J. Hazard. Mater.*, 2009, **161**, 1506–1513.
3 M. Balali-Mood, K. Naseri, Z. Tahergorabi, M. Reza Khazdair and M. Sadeghi, *Front. Pharmacol.*, 2021, **12**, 643972.
4 S. H. Kim, H. Chung, S. Jeong and K. Nam, *J. Cleaner Prod.*, 2021, **279**, 123451.
5 E. Babaei and S. A. Hashemifard, *Sep. Sci. Technol.*, 2021, **57**, 619–636.
6 S. Hussain and S. Ali, *Journal of Ecological Engineering*, 2021, **22**, 104–111.
7 A. Amro, M. Abhary, M. M. Shaikh and S. Ali, *Processes*, 2019, **7**, 406.
8 R. I. A. Ahad, S. Goswami and M. B. Syiem, *3 Biotech*, 2017, **7**, 10.
9 M. Rahimnejad, K. Pirzadeh, I. Mahdavi and S. Peyghambarzadeh, *Environ. Eng. Manage. J.*, 2018, **17**, 1293–1300.
10 M. Mahmoud, M. Osman, O. F. Hafez, A. Hegazi and E. M. Elmelegy, *Desalination*, 2010, **251**, 123–130.
11 Y. Nelson, L. W. Lion, M. Shuler and W. Ghiorse, *Environ. Sci. Technol.*, 2022, **36**, 421–425.
12 X. Zhang, S. Lin, Z. Chen, M. Megharaj and R. Naidu, *Water Res.*, 2011, **45**, 3481–3488.
13 Y. Kobayashi, F. Ogata, C. Saenjum, T. Nakamura and N. Kawasaki, *Water*, 2022, **12**, 2375.
14 M. Q. Chen, J. Liu, Y. Z. Bi, S. Rehman, Z. Dang and P. X. Wu, *J. Hazard. Mater.*, 2020, **388**, 122078.
15 X. F. Feng, R. X. Long, L. L. Wang, C. C. Liu, Z. X. Bai and X. B. Liu, *Sep. Purif. Technol.*, 2022, **284**, 120099.
16 J. Zhu, Z. L. Zhu, H. Zhang, H. T. Lu, W. Zhang, Y. Qiu, L. Y. Zhu and S. Küppers, *Appl. Catal., B*, 2018, **225**, 550–562.
17 Y. C. Dong, X. Y. Kong, X. S. Luo and H. T. Wang, *Chemosphere*, 2022, **303**, 134685.
18 M. D. Xu and M. Wei, *Adv. Funct. Mater.*, 2018, **28**, 2847.
19 H. Bessaha, M. Bouraada and L. Deménorval, *J. Water Reuse Desalin.*, 2017, **7**, 152–161.
20 X. Xie, J. Zhang and L. J. Wang, *Adv. Mater. Res.*, 2014, **1035**, 7–11.
21 Y. Y. Yang, X. F. Tan, E. Almatrafi, S. Ye, B. Song, Q. Chen, H. L. Yang, Q. M. Fu, Y. Deng, Z. T. Zeng and G. Zeng, *Sci. Total Environ.*, 2022, **844**, 156835.
22 R. Soltani, R. Pelalak, M. Pishnamazi, A. Marjani, A. B. Albadarin, S. Sarkar and S. Shirazian, *Sci. Rep.*, 2021, **11**, 1609.
23 F. Y. Lyu, H. Q. Yu, T. L. Hou, L. G. Yan, X. H. Zhang and B. Du, *J. Colloid Interface Sci.*, 2019, **539**, 184–193.

24 Q. Q. Huang, Y. Chen, H. Q. Yu, L. G. Yan, J. H. Zhang, B. Wang, B. Du and L. T. Xing, *Chem. Eng. J.*, 2018, **341**, 1–9.
25 J. H. Zhao, J. Liu, N. Li, W. Wang, J. Nan, Z. W. Zhao and F. Cui, *Chem. Eng. J.*, 2016, **304**, 737–746.
26 M. Xu, H. J. Wang, L. Di, D. Qu, Y. J. Zhai and Y. L. Wang, *J. Environ. Sci.*, 2013, **25**, 479–486.
27 S. B. Tumampos, B. M. B. Ensano, S. M. B. Pingul-Ong, D. C. Ong, C. Kan, J. Yee and M. D. D. Luna, *Int. J. Environ. Res. Public Health*, 2021, **18**, 3050.
28 P. Y. Maneechakr and S. Mongkollertlop, *J. Environ. Chem. Eng.*, 2020, **8**, 104467.
29 K. Y. Meng, X. W. Wu, X. Y. Zhang, S. M. Su, Z. H. Huang, X. Min, Y. G. Liu and M. Fang, *ACS Omega*, 2019, **4**, 18627–18636.
30 M. Q. Xie, X. P. Luo, C. M. Liu, S. H. You, S. Rad, H. J. He, Y. X. Huang and Z. H. Tu, *RSC Adv.*, 2022, **12**, 25833–25843.
31 D. N. Chen, D. G. Li, Z. J. Xiao, Z. Fang, X. G. Zou, P. Chen, T. S. Chen, W. Y. Lv, H. J. Liu and G. G. Liu, *Sci. Total Environ.*, 2021, **773**, 145670.
32 H. Li, Q. Jiang, R. Z. Li, R. W. Zhang, S. M. Jiang, J. X. Zhang, J. H. Qu, L. Zhang and Y. Zhang, *J. Mol. Liq.*, 2022, **353**, 118815.
33 J. Yang, Y. S. Zhang, J. Fu, L. X. Yuan, Z. Li, C. Liu, D. Zhao and X. B. Wang, *Colloids Surf., A*, 2019, **567**, 278–287.
34 A. A. Ichou, R. Benhiti, M. Abali, A. Dabagh, M. Chiban, M. Zerbet, G. Cârjạ and F. Sinan, *Desalin. Water Treat.*, 2020, **178**, 193–202.
35 S. A. Wasay, Md. J. Haron, A. Uchiumi and S. Tokunaga, *Water Res*; , 1996, **30**, 1143–1148.
36 Y. S. Ho and G. S. McKay, *Water Res.*, 2000, **34**(3), 735–742.
37 I. Langmuir, *J. Franklin Inst.*, 1916, **187**, 359–362.
38 H. Freundlich, *Z. Phys. Chem.*, 1907, **57**, 385–470.
39 P. Zhang, W. J. Wang, W. Liu, P. Li, Y. Cai, J. C. Chen and N. S. Ding, *J. Environ. Chem. Eng.*, 2022, **10**, 107751.
40 Y. H. Sun, W. T. Yin, Y. Wang, N. Zhao, X. Y. Wang, J. G. Zhang, Y. R. Guo, S. J. Li and Q. J. Pan, *Chem. Eng. J.*, 2022, **427**, 132017.
41 M. T. Hossain, S. Khandaker, M. M. Bashar, A. Islam, M. Ahmed, R. Akter, A. Alsukaibi, M. D. M. Hasan, H. M. Alshammari, T. Kuba and M. D. R. Awual, *J. Mol. Liq.*, 2022, **368**, 120810.
42 X. Guan, X. Z. Yuan, Y. L. Zhao, J. Bai, Y. Li, Y. X. Cao, Y. Chen and T. Xiong, *J. Colloid Interface Sci.*, 2022, **612**, 572–583.
43 A. Bhattacharya, T. Naiya, S. N. Mandal and S. Das, *Chem. Eng. J.*, 2007, **134**, 529–541.
44 A. Baruah, S. Mondal, L. Sahoo and U. Gautam, *J. Solid State Chem.*, 2019, **280**, 120963.
45 M. S. Mostafa, A. A. Bakr, A. E. E. Naggar and E. A. Sultan, *J. Colloid Interface Sci.*, 2016, **461**, 261–272.
46 L. J. Zhang, Z. S. Ke, W. Z. Wang, H. L. Liu, Y. T. Mao, M. X. Xiang and P. Zhang, *Sep. Purif. Technol.*, 2022, **288**, 120636.
47 Y. Wang and L. Zhang, *J. Colloid Interface Sci.*, 2021, **602**, 469–479.
48 T. L. Hou, L. G. Yan, J. Li, Y. T. Yang, L. J. Shan, X. Meng, X. G. Li and Y. X. Zhao, *Chem. Eng. J.*, 2022, **384**, 123331.
49 X. J. Cheng, J. Q. Deng, X. D. Li, X. D. Wei, Y. N. Shao and Y. L. Zhao, *Chemosphere*, 2021, **287**, 131966.
50 F. Renault, N. Morin-Crini, F. Gimbert, P. Badot and G. Crini, *Bioresour. Technol.*, 2008, **99**, 7573–7586.
51 E. Abu-Danso, S. Peraniemi, T. Leiviska and A. Bhatnagar, *Environ. Pollut.*, 2018, **242**, 1988–1997.
52 W. Ahmed, S. Mehmood, M. Mahmood, S. Ali, A. Shakoor, A. Nunez-Delgado, R. M. A. Asghar, H. Zhao, W. Liu and W. Li, *Environ. Pollut.*, 2023, **326**, 121405.
53 R. R. Shan, L. Yan, K. Yang, Y. F. Hao and B. Du, *J. Hazard. Mater.*, 2015, **299**, 42–49.
54 L. M. Sun, J. S. Wang, J. S. Wu, T. N. Wang, Y. C. Du, Y. L. Li and H. Y. Li, *J. Mater. Sci.*, 2019, **54**, 6882–6894.
55 S. Y. Shi, C. H. Xu, Q. Dong, Y. P. Wang, S. L. Zhu, X. Q. Zhang, Y. Chow, X. Q. Wang, L. Y. Zhu, G. H. Zhang and D. Xu, *Appl. Surf. Sci.*, 2021, **541**, 148379.
56 P. X. Wu, W. Li, Y. J. Zhu, Y. N. Tang, N. W. Zhu and C. Guo, *Appl. Clay Sci.*, 2014, **100**, 76–83.
57 M. Titulaer, J. Jansen and J. Geus, *Clays Clay Miner.*, 1994, **42**, 249–258.
58 H. Yan, W. H. Hu, S. Cheng, H. Xia, Q. Chen, L. B. Zhang and Q. Zhang, *Water Sci. Technol.*, 2020, **82**, 170–184.
59 H. G. Zhou, Z. M. Jiang, S. Q. Wei and J. Liang, *Water, Air, Soil Pollut.*, 2018, **229**, 1–16.
60 N. McIntyre and D. Zetaruk, *Anal. Chem.*, 1977, **49**, 1521–1529.
61 X. F. Liang, Y. Zang, Y. M. Xu, X. Tan, W. Hou, L. Wang and Y. B. Sun, *Colloids Surf., A*, 2013, **433**, 122–131.
62 Y. W. You, H. T. Zhao and G. Vance, *Appl. Clay Sci.*, 2002, **21**, 217–226.
63 X. Xie, J. Zhang and L. J. Wang, *Adv. Mater. Res.*, 2014, **1035**, 7–11.
64 Z. Ni, S. J. Xia, L. G. Wang, F. Xing and G. Pan, *J. Colloid Interface Sci.*, 2007, **3162**, 284–291.